JOURNAL OF GEOPHYSICAL RESEARCH, VOL. 104, NO. A11, PAGES 24,939–24,955, NOVEMBER 1, 1999

Magnetic signatures of the distant polar cusps: Observations by Polar and quantitative modeling

N. A. Tsyganenko [1]

Laboratory for Extraterrestrial Physics, NASA Goddard Space Flight Center, Greenbelt, Maryland

C. T. Russell

Institute of Geophysics, University of California, Los Angeles

Abstract. Polar cusps are an essential element of the magnetospheric topology. In the outermost regions of the cusp the magnetosheath plasma becomes entrained on magnetospheric field lines and penetrates to low altitudes along field lines on the dayside, causing a significant local depression of B, clearly visible in magnetometer data taken at high latitudes. This study addresses the spatial distribution of the magnetic depression associated with the polar cusp, as derived from a large set of Polar magnetometer data taken in 1996-1998. The depression ΔB was derived as the difference between the total magnitude of the observed field and the one calculated from the International Geomagnetic Reference Field model of the internal field, combined with an external field model. In the noon sector the cusp depression is clearly visible in plots of ΔB versus solar magnetic latitude as a relatively narrow region of large negative ΔB (down to ~ -80 nT), extending from $R \sim 8 - 9\, R_E$ (Polar apogee) to $R \sim 5 - 6\, R_E$. At closer geocentric distances the cusp depression fades out because of a rapid increase of the geomagnetic field toward Earth. The cusp depression also shallows as one moves away from the noon meridian and completely disappears at solar magnetic longitudes $\pm 40 - 60°$. The second part of the paper deals with a mathematical representation of the observed polar cusp depression in quantitative models of the geomagnetic field. A method is suggested on the basis of the field deformation technique, making it possible to incorporate a realistic structure of the polar cusps in global models of the magnetosphere.

1. Introduction

The dayside polar cusps are an inherent feature of the outer magnetosphere. Their existence stems from a general topological property of a dipolar magnetic field whose field lines are all confined inside a cavity with a smooth boundary. In all such models, there always exists a pair of points on the boundary where the magnetic field lines bifurcate and the total magnetic field falls off to zero. In the actual magnetosphere this becomes a region of weak field where the geomagnetic field lines are exposed to the oncoming solar wind and thus make it possible for the solar wind plasma to enter into the dayside magnetosphere. A significant flux of particles associated with the dense and relatively cold magnetosheath plasma is therefore observed in the noon sector, localized within a latitudinally narrow magnetic flux tube. The penetration of magnetosheath plasma onto the cusp field lines should result in a significant modification of the original nearly vacuum magnetic field and cause the neutral points to evolve into deep funnel-like diamagnetic structures with a depressed field inside.

The above scenario of the cusp formation and its implications for the magnetospheric magnetic field structure were theoretically predicted in early magnetospheric studies [e.g., *Chapman and Ferraro*, 1931]. Since the beginning of space exploration, a wealth of experimental information on the cusps was obtained, based mainly on low-altitude data on particle fluxes [e.g., *Newell and Meng*, 1988a] and on ground-level auroral observations [e.g., *Sandholt et al.*, 1996]. At larger distances, observations of the cusps were not as numerous as at low altitudes; still, in the first decades of the space era, convincing evidence was found, supporting the earlier theoretical conjectures. *Russell et al.* [1971] showed that the high-altitude cusp was marked by a depressed magnetic field strength and that the southward component of the interplanetary magnetic field (IMF) controlled the location of the cusp. *Fairfield and Ness* [1972] reported a persistent negative anomaly of the distant high-latitude field in the noon sector, associated with the diamagnetic effect of the polar cusp plasma. Later studies, based on data of Hawkeye 1 [*Farrell and Van Allen*, 1990], IMP and HEOS [*Fairfield*, 1991], and Polar [*Zhou et al.*, 1999a] confirmed that a strong

[1] Also at Raytheon ITSS Corporation, Lanham, Maryland.

Paper number 1999JA900279.
0148-0227/99/1999JA900279$09.00

magnetic depression was a characteristic feature of the outer cusp.

In spite of the early appreciation of the complexity of the polar cusp structure and the importance of the penetrating plasma effects, the currently existing magnetic field models do not include the high-latitude diamagnetic depression and represent the polar cusps as an essentially vacuum-like feature of the magnetic field topology with bifurcation points of the field lines in the noon meridian plane.

The purpose of the present work is twofold. First we present results of a detailed study of the northern polar cusp magnetic depression as observed by Polar, after which we describe a simple and convenient method of representing the diamagnetic effect of the polar cusp plasma in global data-based models of the magnetosphere.

2. The Polar Cusp Signatures as Observed by the Polar Magnetic Field Experiment

We used the data of the Polar magnetic field experiment (MFE) [*Russell et al.*, 1995] with 1-min resolution, combined with the 5-min averaged solar wind and IMF data from Wind and IMP 8, using a time shift corresponding to the finite travel distance of the solar wind between the point of measurement and the location of Polar. In total, 32 months of data were used in this study, covering the period between March 20, 1996, and November 30, 1998. The data set of Polar MFE as well as the accompanying interplanetary medium data have been described in detail elsewhere [*Tsyganenko et al.*, 1999], and we do not address them here.

To identify the cusp-related features in the observed structure of the magnetic field, the difference

$$\Delta B = |\mathbf{B}_{\rm obs}| - |\mathbf{B}_{\rm T96}|$$

was calculated between the magnitudes of the observed field $\mathbf{B}_{\rm obs}$ and of the field $\mathbf{B}_{\rm T96}$ given by the data-based model [*Tsyganenko*, 1995, 1996] (T96). The T96 model takes into account the large-scale potential field of the magnetopause currents, which is responsible for the broad vacuum-type depressions of $\mathbf{B}$, associated with the neutral points on the magnetopause. However, the T96 model does not include the effect of the diamagnetic currents in the polar cusp, and it also uses a simplified axially symmetric approximation for the magnetopause, which can result in some underestimation of the contribution of the boundary current to the observed field in the vicinity of the cusps. We therefore expect the difference ΔB to be a convenient indicator of the broad magnetic field depression, associated with the polar cusps and manifested in large negative excursions of ΔB at solar magnetic (SM) latitudes $50^\circ - 80^\circ$ as the spacecraft enters into and exits out of the cusp region.

In general, the shape and position of the polar cusp should depend on the tilt angle Ψ of the Earth's dipole. At ionospheric altitudes, however, both low-latitude data [*Burch*, 1972; *Newell and Meng*, 1989] and models [*Mead and Fairfield*, 1975; *Tsyganenko*, 1976, 1981, 1990; *Stern*, 1985] indicate that the solar magnetic latitude of the cusp footpoint is relatively insensitive to the tilt angle Ψ of the Earth's dipole, so that its average shift between summer ($\Psi \sim 30^\circ$) and winter ($\Psi \sim -30^\circ$) is only $\sim 4^\circ$. The shift can somewhat increase at larger distances; however, owing to the predominance of the dipolar field within $R \leq 8 - 10\,R_E$ on the dayside, one still can assume that the position of the distant polar cusps approximately follows the orientation of the geodipole axis (i.e., remains nearly fixed in the SM coordinates). For that reason, we chose the SM coordinate system as a natural one for organizing the dayside data. To further decrease the scatter due to the difference in the tilt angle values for individual data, we binned them into four intervals of Ψ.

As discussed below, the amplitude of the depression depends on the magnitude of the field just outside the polar cusp, and, since that field rapidly increases earthward, we binned the data into four intervals of the geocentric distance, $8 < R \leq 9\,R_E$, $7 < R \leq 8\,R_E$, $6 < R \leq 7\,R_E$, and $5 < R \leq 6\,R_E$, and studied them separately. Because of the high inclination of the Polar orbit and the larger speed of the spacecraft at closer distances, the number of data points rapidly decreased toward Earth, which is why no sensible results could be obtained for $R \leq 5\,R_E$.

2.1. Radial and Latitudinal Distribution of the Cusp-Related Depression Near Noon

Since the polar cusps are located near the noon meridian plane, one should expect that the effect of the depression peaks in that region. To better resolve the spatial distribution of the cusp depression, we left out data taken too far from noon when creating the data set. At an early stage of this work the data were binned with respect to the solar magnetic (SM) longitude, and distributions of ΔB were plotted for each interval of R as functions of the SM latitude. However, it was then realized that, because of the convergence of the longitude sectors near the polar axis, the amount of data in the latitude bins significantly decreased as the latitude approached 90°.

To retain decent coverage in the interesting region near the polar axis, we chose to bin the data using a different spherical coordinate system, in which the polar axis coincided with the $X_{\rm SM}$ axis and the data were selected from a narrow (20°-wide) sector of the angle $\phi = \arctan(Y_{\rm SM}/Z_{\rm SM})$, centered on the SM noon meridian plane, as shown in Figure 1. The observed values of ΔB were then binned into 2° intervals of the angle θ, measured from the positive direction of the $X_{\rm SM}$ axis.

It is known [*Tsyganenko and Usmanov*, 1984; *Newell et al.*, 1989; *Zhou et al.*, 1999b] that the longitudinal position of the cusps is affected by the IMF B_y component. To reduce possible scatter from that effect, only data with IMF $|B_y| \leq 3$ nT were retained in the set.

Figure 2 displays a distribution of the values of ΔB against θ for the outermost interval, $8 < R \leq 9\,R_E$, of the radial distance, covered by the data of Polar. The upper row of plots shows the data obtained during northward IMF conditions, and the lower one is for southward IMF. In each row, four plots, from left to right, correspond to four intervals of the geodipole tilt angle, indicated above each plot. A well-pronounced depression, localized around $\theta \sim 60^\circ - 75^\circ$, can be clearly seen in all eight plots, which means that the actual cusp depression is stronger and extends much closer to Earth than predicted by the T96 model.

Note that the data shown in these plots were taken by the spacecraft near apogee, where its speed is minimal and hence

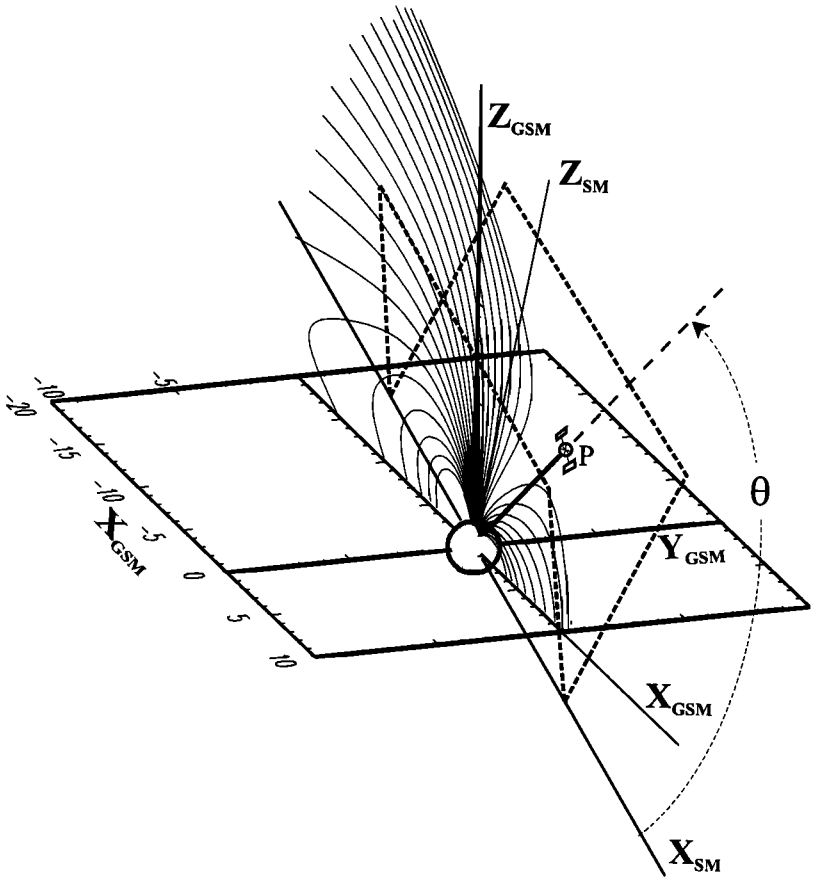

Figure 1. Illustration of the coordinates used in the selection of the data. The letter P indicates the position of Polar.

the data coverage is the best, with the total number of points between 8846 and 19,751. Nonetheless, because of orbital limitations, in most plots the data still do not fully cover the cusp depression, and the numbers of data points in individual bins of θ vary within wide limits (indicated by a gray-scaled shading). The widest coverage was obtained for the second and third intervals of the tilt angle (between $-15°$ and $+15°$), while in the case of the most positive tilt angles ($15° < \Psi \leq 35°$), there are no data for latitudes equatorward of $\sim 60°$.

Three interesting features should be noted. First, there is no dramatic difference in the depression strength between the northward (top row) and southward (bottom row) IMF conditions. Although the peak amplitudes of ΔB appear somewhat larger for negative IMF B_z, in most cases the difference does not exceed the rms scatter within individual bins of θ, or else no comparison can be made at all because of incomplete latitudinal coverage (especially for large absolute values of the tilt angle at large radial distances, as can be seen in Figure 2).

Second, a region of positive ΔB exists poleward of the negative depression, becoming more pronounced as the tilt angle changes from negative to positive values. This feature (absent in the following plots for smaller radial distances) can be interpreted as evidence of an enhanced compression of the magnetic field due to a local increase of the angle of incidence of the solar wind poleward from the center of the cusp "funnel," as schematically illustrated in Figure 3. In a recent work, *Sotirelis and Meng* [1999] predicted the same effect on the basis of their results of a calculation of the magnetopause shape, satisfying the condition of the pressure balance between the T96 magnetic field and the solar wind.

Third, since the summer cusp is more exposed to the solar wind than the winter one [*Newell and Meng*, 1988b], one might expect stronger depressions in the northern cusp for positive tilt angles. Although this feature is rather obscure in Figure 2 (which may be due to insufficient latitudinal coverage at large tilt angles), it becomes more pronounced at closer radial distances, as we will see below in Figures 4–6.

It is also worth noting here that the actual latitudinal width of the diamagnetic depression associated with the cusp plasma is probably significantly smaller than in the average statistical patterns in Figure 2. *Zhou et al.* [1999a] used a similar method of detrending the polar cusp signatures by subtracting the T96 model field from Polar MFE data. They have found that typical profiles of ΔB in individual crossings consisted of broad, smooth, and relatively shallow depressions, with an additional abrupt decrease of ΔB in the middle, associated with simultaneous sudden increase in the low-energy ion and electron density and enhanced magnetic noise (see their Figure 1). Such a structure can be explained as a combined effect of two sources: the narrow dip in the center is due to the diamagnetic currents proper, while the broader smooth depression results from inaccurate description of the model magnetopause in the vicinity of the cusps. More specifically, as illustrated in Figure 3 (right), the T96

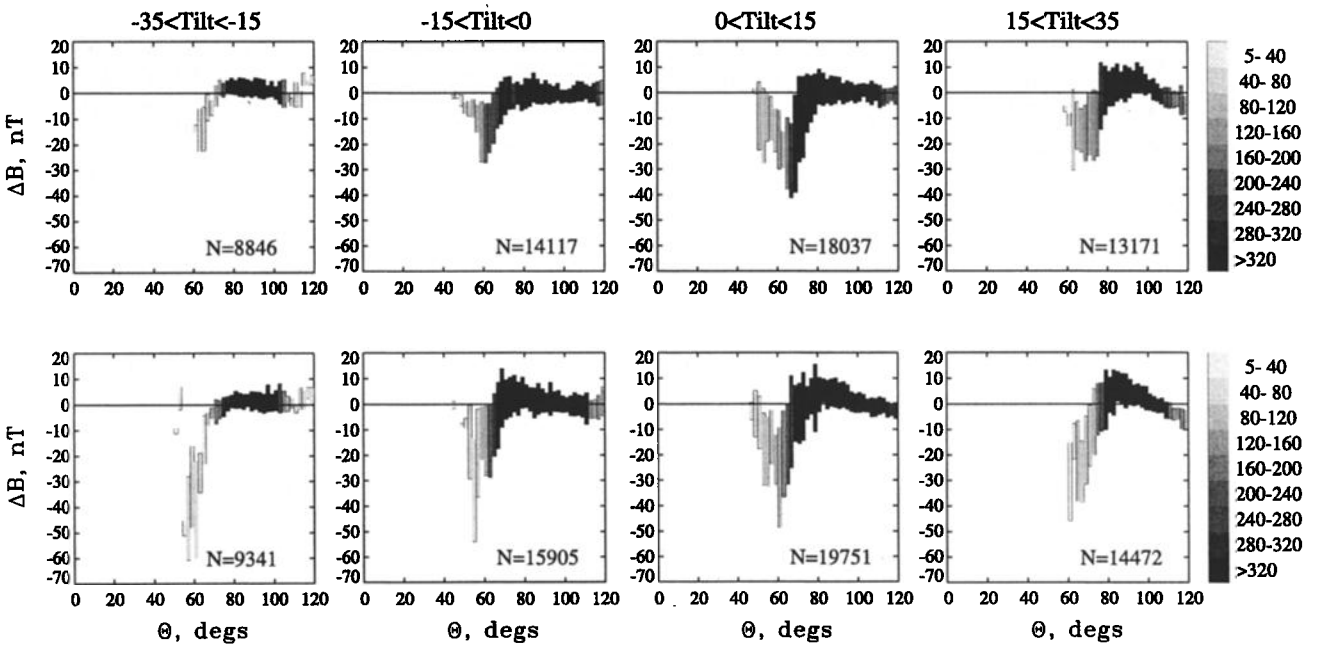

Figure 2. Distribution of the difference ΔB between the scalar magnitudes of the magnetic field measured by Polar and of that predicted by T96 model, plotted against the angle θ (Figure 1) for (top) positive and (bottom) negative polarities of the IMF B_z and for four intervals of the dipole tilt angle, as indicated (in degrees) above each column. Centers of the shaded strips indicate average values, and their heights correspond to the rms deviation of ΔB for each bin of θ, while the intensity of the gray-scale shading is proportional to the number of 1-min averages in each bin, according to the densitometer bar on the right. This plot corresponds to the farthest bin of the radial distance, $8 \leq R < 9\ R_E$. Note a conspicuous positive excursion of ΔB polarward from the depression, due to enhanced ram pressure of the magnetosheath plasma flow in that region.

model uses a smooth axially symmetric boundary, whereas the actual magnetopause is indented near the cusps and hence the actual boundary currents are stronger and located closer to Earth than those of the model. This results in a stronger northward field of the boundary currents and hence in a deeper depression than predicted by the T96 model.

Figure 4 displays the distribution of ΔB for a closer distance, $7 < R \leq 8\ R_E$, in the same format as in Figure 2. In this case the numbers of data points are 3–4 times smaller than in Figure 2. Nonetheless, the localized depression of ΔB is again clearly visible, and clear trends can be seen with regard to its dependence on the tilt angle and IMF B_z. However, as already noted, the positive "anomaly" of ΔB, quite conspicuous in all plots of Figure 2 for the outermost interval of R, is virtually absent in this case.

The next eight plots shown in Figure 5 display the results

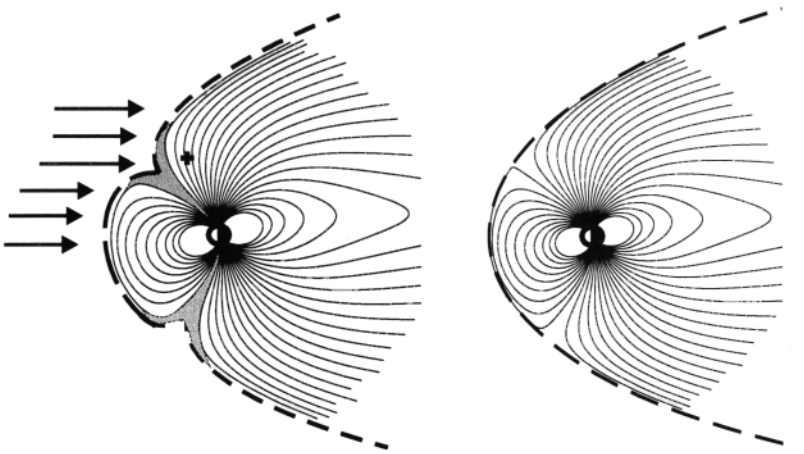

Figure 3. Illustration of the difference between the polar cusp structure (right) in an idealized model and (left) in the actual magnetosphere. Injection of the magnetosheath plasma results in a weaker magnetic field inside the polar cusps (gray shading), as compared to that in the vacuum-type model, while the indented shape of the boundary results in an enhanced field in the vicinity of the Polar apogee (marked by a cross).

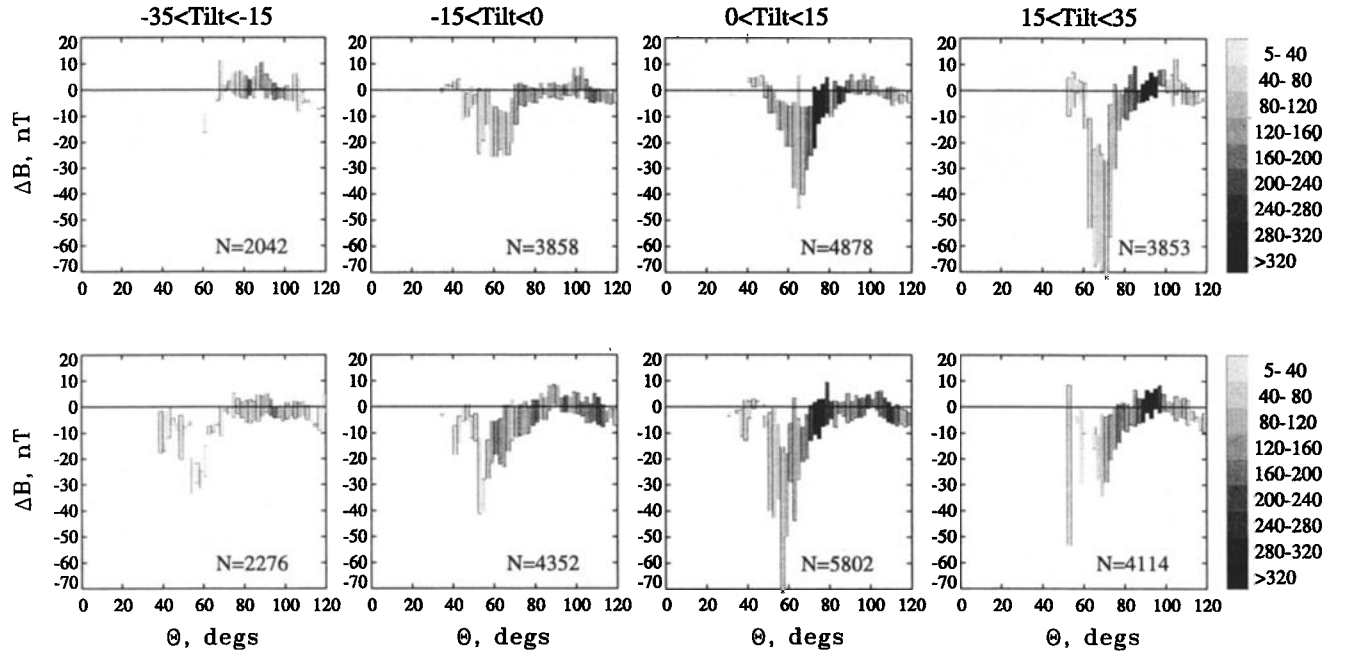

Figure 4. Distribution of ΔB for $7 \leq R < 8\ R_E$, in the same format as in Figure 2.

for even closer distances: $6 < R \leq 7\ R_E$. While the numbers of the data points further drop by a factor of $\sim$ 2–3 and the structure of ΔB becomes more irregular owing to poorer statistics, one still can easily discern clear minima associated with the polar cusps, whose amplitude generally increases as we proceed from winter to summer conditions. In the second and third plots in the bottom row (for IMF $B_z < 0$) a double-peaked depression can be seen. An inspection of the data showed that in both cases the low-latitude peaks corresponded to isolated events with a large negative IMF B_z and a very strong dynamic pressure of the solar wind.

In the last set of the plots in Figure 6, corresponding to the innermost bin of radial distances, $5 < R \leq 6\ R_E$, the depression is shallower than at higher altitudes and spread out over larger intervals of latitudes. The data coverage in this case is even scanter: many of the latitude bins are empty, and most of the others contain 1-min data taken during a single pass of Polar.

2.2. Longitudinal Extent of the Polar Cusp Depression

The question of the azimuthal extension of the polar cusps is an interesting and important one, raised in the literature

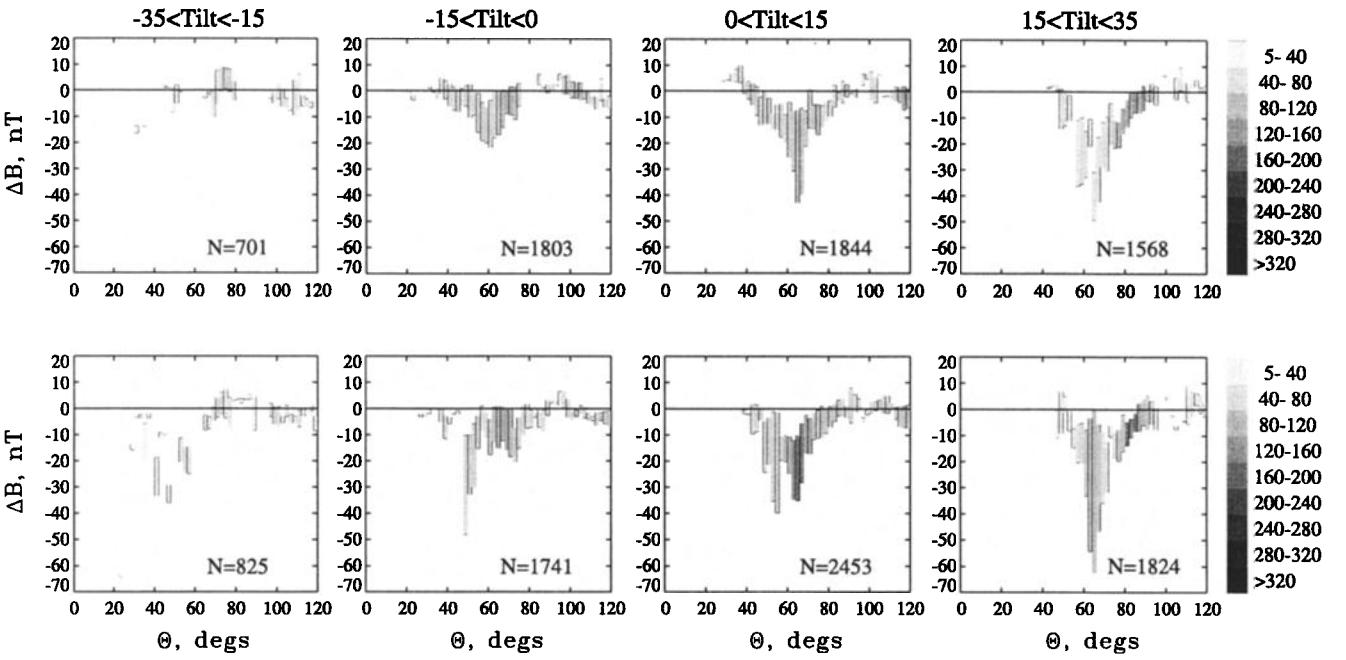

Figure 5. Distribution of ΔB for $6 \leq R < 7\ R_E$, in the same format as in Figure 2.

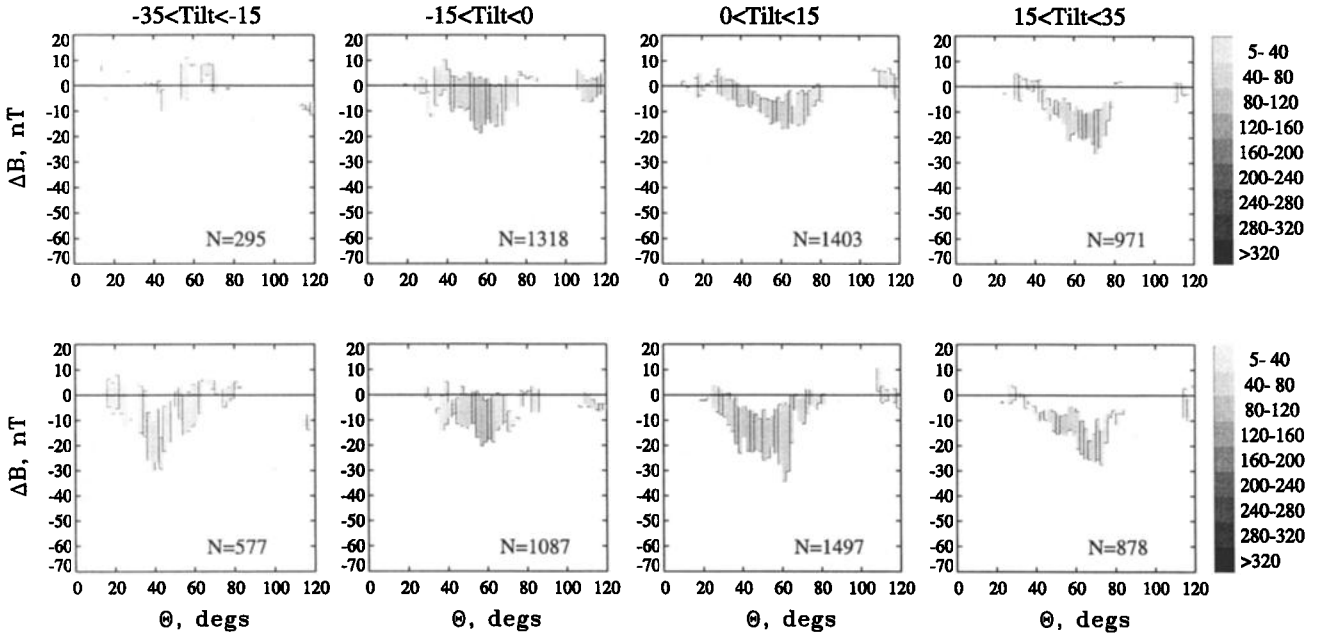

Figure 6. Distribution of ΔB for $5 \leq R < 6\ R_E$, in the same format as in Figure 2.

since early days of the magnetospheric physics. A detailed historical overview of studies of the polar cusp geometry as seen by low-altitude particle observations was given by *Newell and Meng* [1988a]; in the same paper the azimuthal extension of the polar cusps was quantitatively described in terms of the probability of their detection at various magnetic local times. According to those results, the characteristic width of the cusp at an altitude of $\sim$ 800 km is 3-4 hours of local time.

Much less is known on the azimuthal extension of the cusps at higher altitudes. Back in the 1960s, a conjecture was made [e.g., *Walters*, 1966] that the dayside neutral points on the magnetopause extended on the nightside as two demarcation lines between the closed low-latitude field lines and the high-latitude field lines, which stretched to the nightside and merged on the flanks of the tail plasma sheet. Quite recently, that concept was revived in the so-called "magnetospheric sash," a band of weak magnetic field connecting the outer dayside cusps with the cross-tail current sheet and observed in an MHD simulation [*White et al.*, 1998].

In this work we address the problem from the viewpoint of the magnetic field observations. Again, the data were binned into two subsets, for positive and negative IMF B_z, respectively, and in order to reduce the scatter due to the IMF-induced shift of the cusp in the east-west direction, only data with IMF $|B_y| \leq 3$ nT were retained. In addition, only data with relatively small values of the dipole tilt angle, $|\Psi| \leq 10°$, were selected, in order to reduce the seasonal/diurnal effects. Only the outermost intervals of the radial distance were analyzed in this case: $7 < R \leq 8\ R_E$ and $8 < R \leq 9\ R_E$. Finally, in this part of the study we concentrated primarily on the longitudinal variation of the cusp depression, while effects near the SM polar axis were considered of secondary importance. For that reason, the data were binned here into intervals of the SM longitude λ, rather than of the angle θ, as in section 2.1.

More specifically, the data were binned into three groups, corresponding to three intervals of the absolute value of the SM longitude λ: (1) $|\lambda| \leq 20°$, (2) $20° < |\lambda| \leq 40°$, and (3) $40° < |\lambda| \leq 60°$. Thus each group included observations made within two sectors of SM longitude, positioned symmetrically with respect to the noon meridian. Such a binning implies a dawn-dusk symmetry of the cusps, which was expected owing to the selection of data with IMF $|B_y| < 3$ nT.

Figure 7 shows the plots of $\Delta B = |\mathbf{B}_{obs}| - |\mathbf{B}_{T96}|$ against the SM latitude for three intervals of $|\lambda|$ and for both polarities of the IMF B_z. This plot corresponds to $7 < R \leq 8\ R_E$. As expected, the depression is greatest in the noon sector, but it is much smaller for $20° < |\lambda| \leq 40°$, and it almost disappears for $40° < |\lambda| \leq 60°$. Figure 8 shows in a similar format the results for the most distant bin of the radial distance, $8 < R < 9\ R_E$. Here one still can see a few points with a relatively large $|\Delta B|$ even in the bin $40° < |\lambda| \leq 60°$, farthest from noon.

The following conclusions can be made from these plots: (1) the longitudinal extent of the polar cusp depression at $7 < R < 9\ R_E$ is about 2 hours of local time in both directions away from noon; (2) the azimuthal extent of the depression appears to increase with growing distance, which may corroborate the concept of the "sash."

3. Modeling of the Polar Cusp Structure

This section outlines an analytical method, allowing one to incorporate the observed structure of the polar cusps in any quantitative model of the geomagnetic field. The method is based on the deformation technique, suggested by *Stern* [1987] and further developed by *Tsyganenko* [1998].

3.1. Modeling Method

The basic idea is to introduce a local rarefaction of the magnetic flux inside a limited region of space on the dayside, corresponding to the location of the polar cusp field lines. It

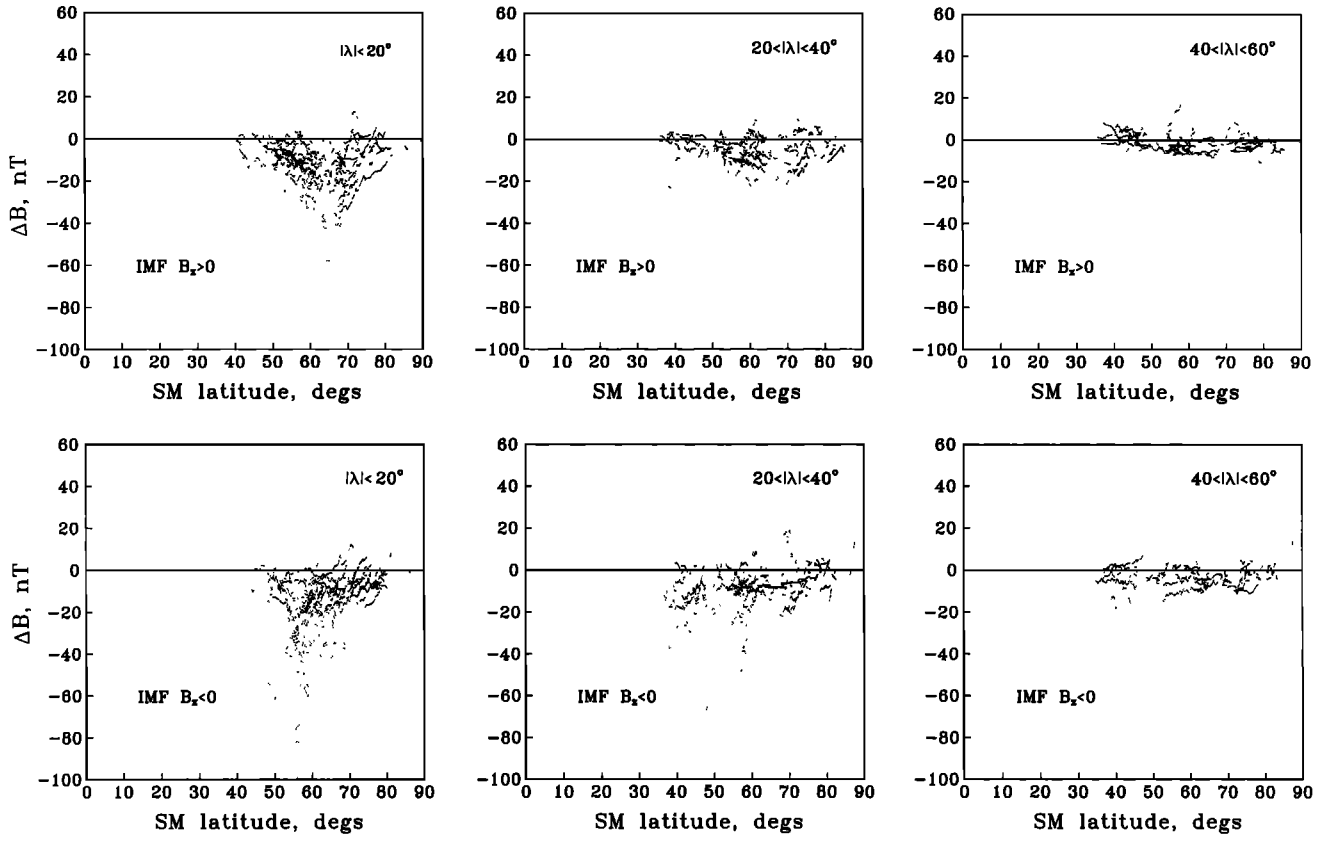

Figure 7. Illustration of the azimuthal distribution of the polar cusp depression. Individual values of $\Delta B = B_{\text{obs}} - B_{\text{model}}$ are plotted against the solar magnetic (SM) latitude for three intervals of the absolute value of the SM longitude λ (from left to right) and for two polarities of the IMF B_z (positive in the top and negative in the bottom). A clear decrease of ΔB with increasing $|\lambda|$ can be seen for both IMF B_z polarities. This plot corresponds to small values of the Earth's dipole tilt ($-10° \le \Psi \le +10°$) and for $7 \le R < 8\ R_E$.

is intuitively clear that the desired effect can be obtained by a modification ("stretching") of a coordinate whose variation shifts field lines nearly orthogonally to their local direction. In a rough approximation the magnetic field in the polar cusp field line tube is nearly radial, and hence we could try to stretch the solar magnetic latitude. However, that choice is not quite convenient because the cusps are located relatively close to the polar axis and lack axial symmetry. In addition, as we have seen in Figure 2, effects of solar wind pressure can extend poleward well beyond the cusps and remain significant near the polar axis. With spherical coordinates, overcoming these problems would be mathematically cumbersome. An additional complication would also arise owing to the singularity of spherical scale factors on the polar axis.

A much more convenient choice is to use a cylindrical coordinate system $\{\rho, \phi, Y\}$ whose Y axis coincides with the solar magnetic Y_{SM} axis and where the coordinate to deform is the azimuthal angle ϕ, measured sunward from the positive direction of the Z_{SM} axis, as schematically illustrated in Figure 9. Using the cylindrical coordinates fits well our finding, discussed in the previous section, that the polar cusp depression has a limited extent in the longitudinal direction. Owing to that fact, the coordinate Y can be used for representing the longitudinal variation of the cusp field not far from the noon meridian plane, while the angle ϕ approximately equals the SM colatitude in that region.

A formal deformation of the angular coordinate, $\phi \Rightarrow F(\rho, \phi, Y)$, entails the following transformation of the magnetic field components [*Tsyganenko*, 1998]:

$$B'_\rho = B^*_\rho \frac{\partial F}{\partial \phi},$$
$$B'_\phi = B^*_\phi - \rho\left[B^*_Y \frac{\partial F}{\partial Y} + B^*_\rho \frac{\partial F}{\partial \rho}\right], \qquad (1)$$
$$B'_Y = B^*_Y \frac{\partial F}{\partial \phi},$$

where the asterisks denote "mapped" components; that is, $B^*_{\rho,\phi,Y} \equiv B_{\rho,\phi,Y}(\rho, F, Y)$.

It is convenient to define the deformed azimuthal coordinate F as a sum of the undeformed one ϕ and of a perturbation term

$$F = \phi + af(\rho, Y)\,\Lambda(\phi - \phi_c, \delta\phi). \qquad (2)$$

The variation of the perturbation term of (2) in the radial and east-west directions is given by the factor $f(\rho, Y)$, while the dependence on the angle ϕ is represented by the function $\Lambda(\phi - \phi_c, \delta\phi)$. According to (1), the magnetic field strength inside the cusp (defined mainly by the B_ρ component) is approximately proportional to the derivative $\partial F/\partial\phi$. Therefore the factor Λ should be defined in such a way that $\partial F/\partial\phi$ has

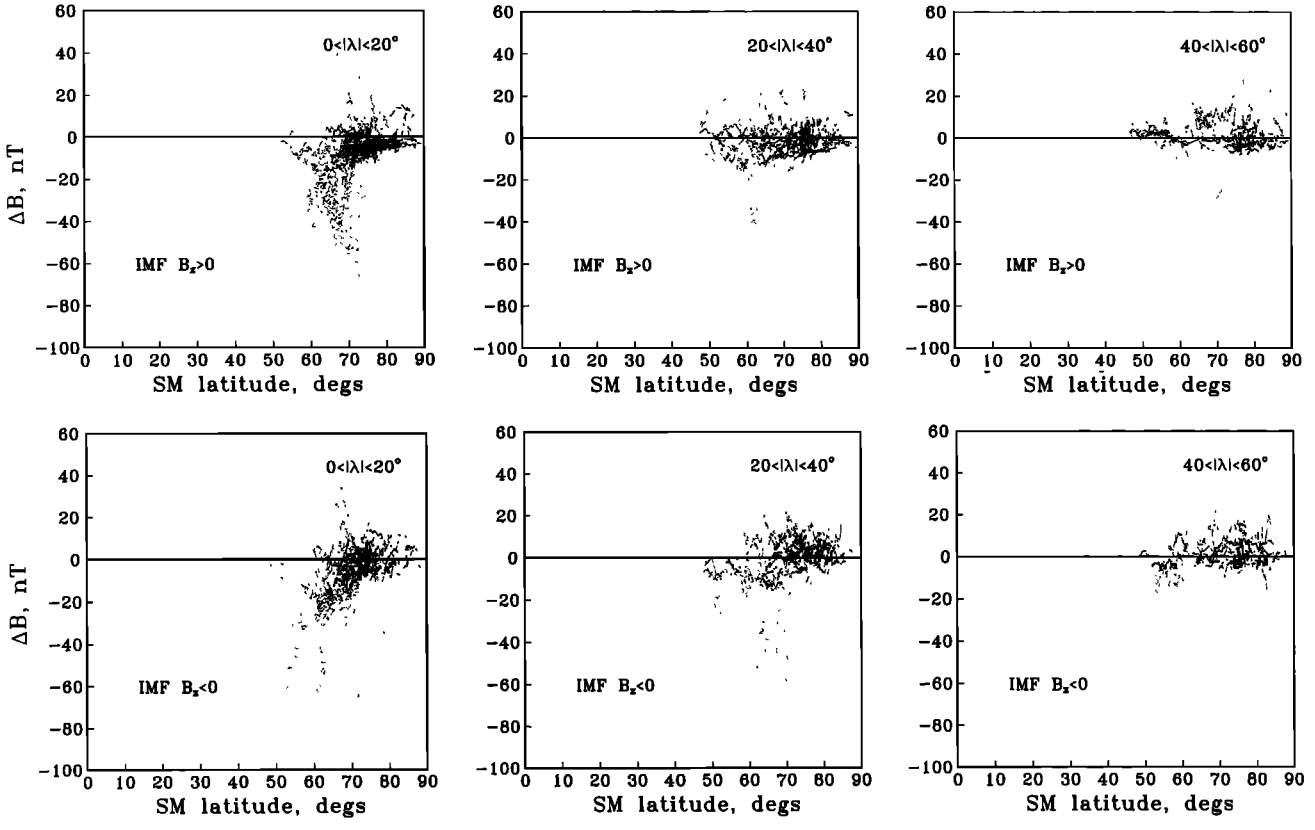

Figure 8. Illustration of the azimuthal distribution of the polar cusp depression. This plot corresponds to $8 \leq R < 9\ R_E$, and the data format is similar to that in Figure 7.

a local dip in a vicinity of the cusp, extending over a characteristic angular width $\delta\phi$, with its minimum at $\phi = \phi_c$. Note that both ϕ_c and $\delta\phi$ are functions of ρ, so that the angular position and width of the polar cusp depression can be made to match its observed shape. The angle ϕ_c should also depend on the dipole tilt angle; a specific form of that dependence will be given below.

To simplify the description of the angular variation $\Lambda(\phi - \phi_c, \delta\phi)$ of the perturbation term in more detail, let us temporarily denote $\phi - \phi_c \equiv \omega$. As already said, in the vicinity of the cusp, $|\omega| \leq \delta\phi$, the perturbation term should provide a local decrease of $\partial F/\partial\phi$, which can be achieved by choosing the function $\Lambda(\omega, \delta\phi)$ as shown in Figure 10 (the factor $af(\rho, Y)$ will be negative). Inside the cusp, $\Lambda(\omega, \delta\phi)$ is a locally linear function with a positive slope, while for $|\omega| \geq \delta\phi$ it smoothly falls off to zero.

It is convenient to normalize the function Λ so that for any value of the characteristic angular variation scale $\delta\phi$,

$$\left.\frac{\partial\Lambda}{\partial\omega}\right|_{\omega=0} = 1\,. \tag{3}$$

This allows one to easily control the depth of the field depression as a function of ρ and Y by specifying the factor $f(\rho, Y)$ and the overall disturbance amplitude a in (2). If $-1 < af < 0$, then $0 < \partial F/\partial\omega < 1$, which corresponds to a depressed field magnitude inside the cusp.

Outside of the cusp the perturbation results in a slight increase of the magnetic field, because of the added magnetic flux, displaced from inside the cusp. Owing to a narrow angular width of the cusp depression, the displaced flux is relatively small, and, since it is distributed over a large interval $\delta\phi \leq \omega \leq \pi$, the resultant increase of the outer field is, generally, much smaller than the disturbance inside the cusp.

If the function Λ is antisymmetric with respect to ω (i.e., is an odd function), then the field increases evenly on both sides of the cusp. In the outer cusp, however, we need to replicate the observed asymmetric deformation so that the field on the poleward side of the northern cusp "funnel" will be more compressed than on the equatorward side, as suggested by data (Figures 2 and 3). This can be easily achieved by introducing asymmetry in the angular deformation Λ with respect to the cusp center $\omega = 0$, as shown in Figure 10 (bottom). Other than the above requirements, the function Λ should also be continuous with its derivative $\partial\Lambda/\partial\omega$ in the entire range $-\pi \leq \omega \leq \pi$.

A simple analytical form satisfying all these criteria and the normalization condition (3) can be chosen as

$$\Lambda = \frac{C\delta\phi}{C - \delta\phi}\left[\Theta\left(1 + \frac{\omega}{S}\right)\exp\left(\frac{\delta\phi - S - \omega}{C}\right)\right.$$
$$\left.-(1 - \Theta)\left(1 - \frac{\omega}{S}\right)\exp\left(\frac{\delta\phi - S + \omega}{C}\right)\right]\cos\frac{\omega}{2}\,, \tag{4}$$

where $S = \sqrt{\omega^2 + \delta\phi^2}$. The parameter C is an e-folding an-

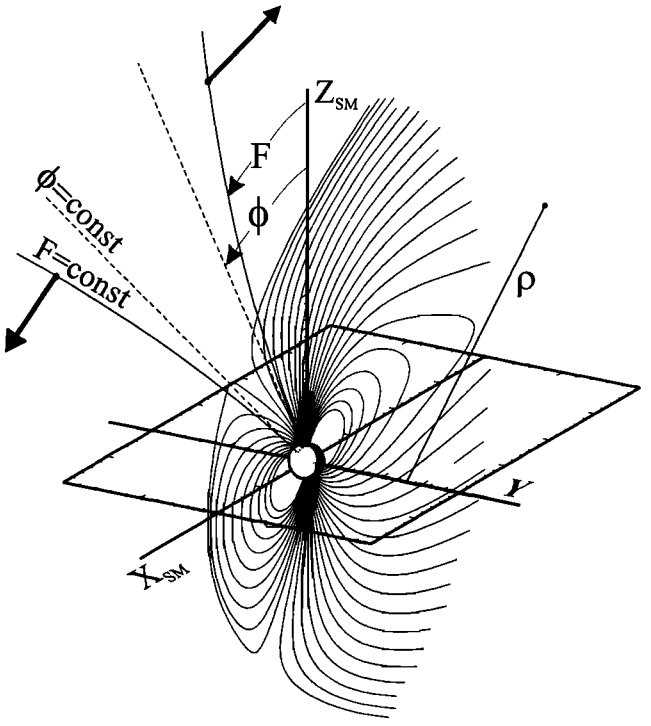

Figure 9. Deformation of the coordinates given by equations (1) and (2), devised for representing the diamagnetic effect of the polar cusp plasma. The angle ϕ undergoes a stretch, directed away from the local position of the center of the polar cusp (shown by arrows). The amplitude of the deformation varies with the distance ρ from the Y axis and is maximal in the noon meridian plane.

gular distance, defining the rate at which the field disturbance falls off away from the cusp. The parameter Θ controls the asymmetry of that disturbance, so that $\Theta = 0.5$ corresponds to a symmetric case (approximating observations in the inner cusp), while $0 \leq \Theta < 0.5$ yields a larger positive ΔB poleward from the cusp, allowing one to simulate the observed asymmetry in the compression of the high-latitude magnetic field on the dayside. The factor $\cos(\omega/2)$ ensures a smooth behavior of the perturbation term and its derivatives at $\omega = \pm\pi$. Figure 10 shows three sample plots of the function Λ for different values of the parameters.

The function ϕ_c, giving the shape of the polar cusp in the noon meridional cross section, is defined from the following considerations. At close geocentric distances the line $\phi = \phi_c(\rho)$ should approximately match the shape of a dipolar field line with the footpoint latitude of $75° - 78°$, while at large distances it should pass in the vicinity of the cusp depression, observed by Polar, and it also should match the position of the dayside neutral points as obtained in the models. A simple form for $\phi_c(\rho)$ can be adopted from the Region 1 Birkeland current sheet model developed by *Tsyganenko and Stern* [1996]. Following that approach, we specify the angular position of the cusp as a function of the distance ρ as

$$\phi_c = \arcsin \frac{\sqrt{\rho}}{\left(\rho^{\beta} + \sin^{-2\beta}\phi_{c0} - 1\right)^{\frac{1}{2\beta}}}, \qquad (5)$$

where the parameter ϕ_{c0} is the angular position (colatitude) of the cusp footpoint at the noon meridian and β is a parameter. As required, at low altitudes ($\rho \sim 1$), (5) yields $\sin^2\phi_c \approx \rho \sin^2\phi_{c0}$, that is, cusp field lines are nearly dipolar, while in the limit of very large distances $\phi_c \to \pi/2$. An inspection of the cusp shapes given by (5) with different values of the parameter β was made. Having compared them with the shapes of the cusp magnetic field lines in the T96 model, we found that the value $\beta = 1$ provided the best approximation.

To incorporate the effects of the dipole tilt upon the position of the cusps, the adopted form of ϕ_c can be easily modified as follows. First, as already noted in section 2, in a rough approximation the polar cusps tilt in the GSM coordinates in

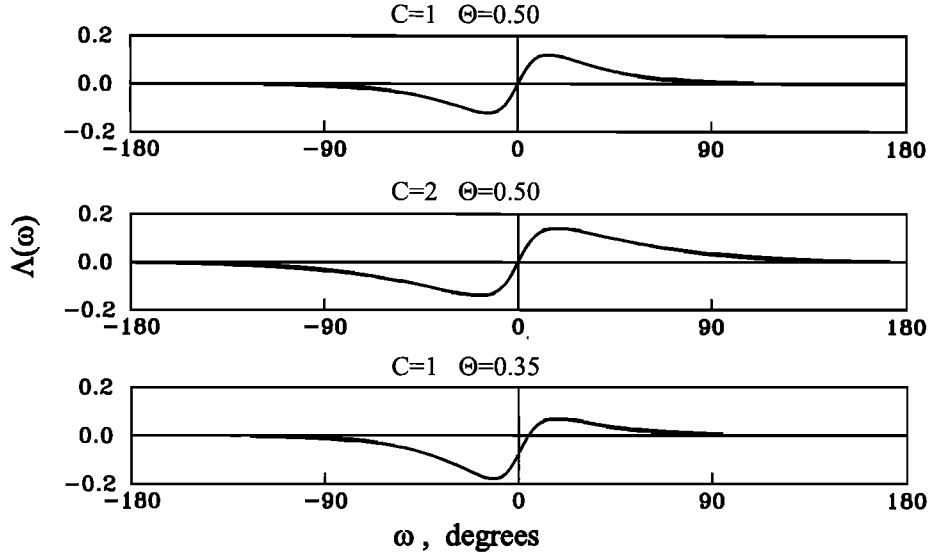

Figure 10. Plots of the function $\Lambda(\omega)$ for three sets of the parameters: (top) a symmetrical deformation ($C = 1$ and $\Theta = 0.5$); (center) a symmetrical deformation with a more uniform distribution of the displaced magnetic flux outside of the cusp ($C = 2$ and $\Theta = 0.5$); and (bottom) asymmetrical deformation with a stronger field on the poleward side of the cusp ($C = 1$ and $\Theta = 0.35$).

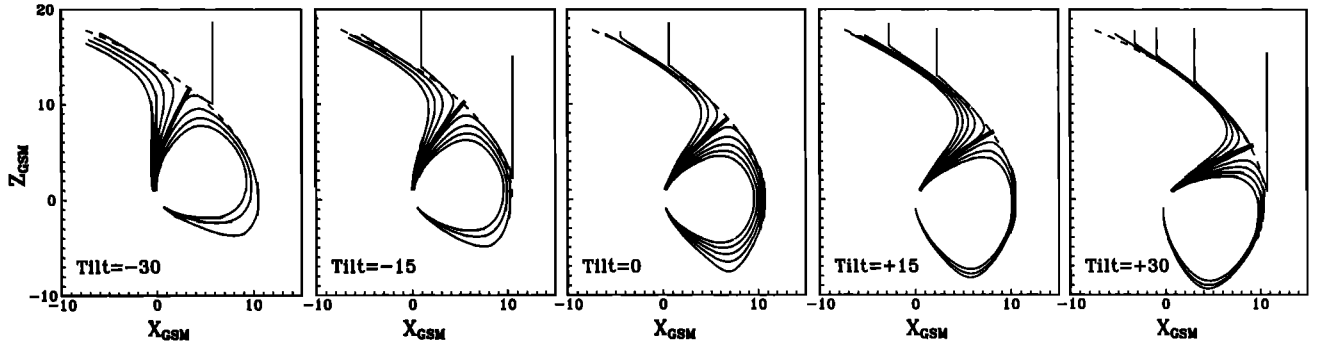

Figure 11. Variation of the shape and position of the polar cusp with the dipole tilt angle, as approximated by equations (5)–(7). The centerline of the model cusp is shown by a thick solid line.

concert with the Earth's dipole, that is, by the same angle Ψ, as if they were rigidly fixed with respect to the dipole axis. In a more accurate treatment one should include a relatively small slippage so that for the solstice conditions with $\Psi \sim \pm 30°$ both northern and southern cusp footpoints shift by the same amount in the direction opposite to the dipole tilt. In the next approximation one must include the even finer effect of the difference between the shift amplitudes in the opposite hemispheres.

The above considerations prompt a simple generalization of (5), providing the tilt-dependent shape and position of the cusp via the angle ϕ_c:

$$\phi_c = \arcsin \frac{\sqrt{\rho}}{\sqrt{\left(\rho + \sin^{-2}\phi_1 - 1\right)}} + \Psi\,, \qquad (6)$$

where

$$\phi_1 = \phi_{c0} - (\alpha_1 \Psi + \alpha_2 \Psi^2)\,. \qquad (7)$$

Adding the tilt angle Ψ to the first term in the right-hand side of (6) makes the cusp rotate (tilt) with the dipole, while the additional linear and quadratic terms in the right-hand side of (7) describe the above discussed first- and second-order effects of the slippage of the cusp footpoints.

Numerical values of the parameters α_1 and α_2 can be found either from low-altitude data on the cusp particles or by tracing field lines using data-based magnetic field models and by adjusting the cusp footpoints to match the projections of the dayside quasi-neutral points on the ionosphere. In this work the second approach was used. Figure 11 shows five meridional sections of the dayside model magnetosphere for $\Psi = -30°$, $\Psi = -15°$, $\Psi = 0°$, $\Psi = 15°$, and $\Psi = 30°$, each with a family of near-cusp field lines, obtained using the T96 model with $p_{\rm dyn} = 3$ nPa, $Dst = -20$, IMF $B_y = 0$, and $B_z = -2$ nT. For that particular set of model parameters, the numerical values of the angle ϕ_{c0} and of the coefficients α_1 and α_2 in (6)–(7) were found to be equal to 0.24, 0.1287, and 0.0314, respectively (assuming all the angles in (6)–(7) to be given in radians). The shape and position of the polar cusps (shown in each of the plots by a thick solid line) quite accurately match the shape of the cusp field lines and their bifurcation points at the magnetopause.

So far, we have considered the tilt angle effect upon the geometrical characteristics of the polar cusp. Besides that, as already noted in section 2, there exists a significant modulation by the dipole tilt angle of the diamagnetic depression owing to the varying degree of the cusp exposure to the magnetosheath plasma flow. This effect should also be represented in the model, and the simplest way is to introduce a tilt dependence in the amplitude factor of the deformation function.

With all of the above in mind we rewrite the total deformation (2) of the angle ϕ in a form including both northern and southern polar cusps and taking into account all symmetry properties:

$$F = \phi + f(\rho, Y)\Big[a(\Psi)\Lambda\big(\phi - \phi_c(\rho, \Psi), \delta\phi\big) - a(-\Psi)\Lambda\big(\pi - \phi - \phi_c(\rho, -\Psi), \delta\phi\big)\Big]\,, \qquad (8)$$

where $\phi_c(\rho, \Psi)$ is defined by (6)–(7) and the amplitude $a(\Psi)$ can be assumed, for simplicity, as a linear function of the tilt angle: $a(\Psi) = a_0 + a_1\Psi$.

The next step is to specify the radial and azimuthal distribution of the cusp-related disturbance by choosing the function $f(\rho, Y)$. The observed spatial extent of the cusp depression in the dawn-dusk direction, as described in section 2, was found to be relatively small, which allowed us to use the cylindrical coordinates. We chose a simple Gaussian profile for the variation of the cusp disturbance along the Y direction, centered on the noon meridian plane and confined within a limited interval of longitude. As for the radial variation, one can expect the disturbance to rapidly fall off toward Earth because of a steep increase of the background magnetic field. A more quantitative treatment of this question is as follows.

The ratio of the magnitude of the perturbed model field inside the cusp to the background exterior field B_e at the same radial distance outside the cusp can be approximately evaluated from (1)–(3) as

$$\frac{B}{B_e} \approx \frac{B'_\rho}{B^*_\rho} = \frac{\partial F}{\partial \phi} = 1 + af(\rho, 0)\,.$$

On the other hand, assuming for a moment that the plasma pressure p in the distant cusp is isotropic (and hence, by Liouville's theorem, remains isotropic throughout the entire

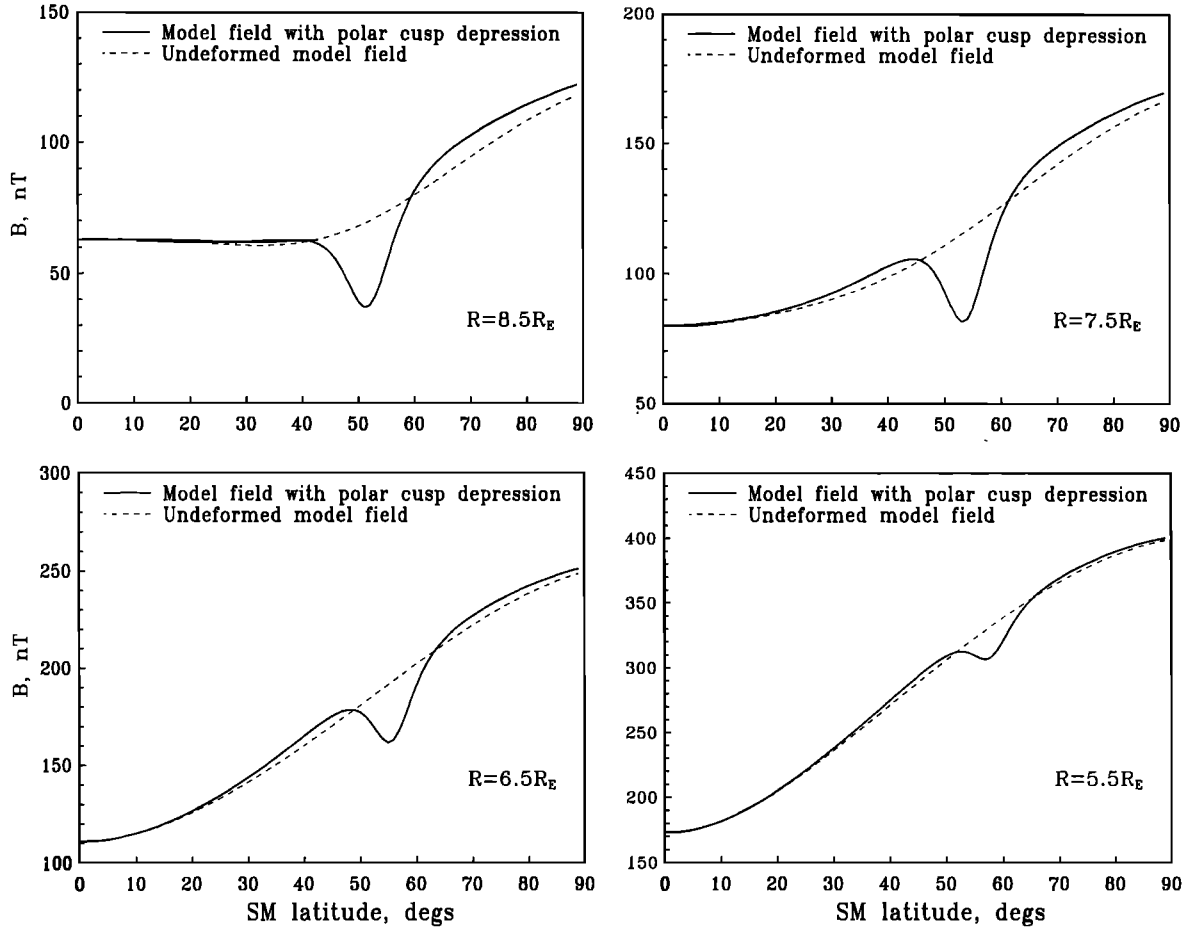

Figure 12. Variation of the total magnetic field across the model cusp for four values of the radial distance, plotted as a function of SM latitude in the noon meridian plane. The dashed line corresponds to undeformed model field, and the solid line includes the effect of the polar cusp depression, modeled by using the deformation method. The plots do not represent any fitting to actual data and are intended only for illustrating the method.

cusp), one can derive the same ratio from the equation of the transverse pressure balance as

$$\frac{B}{B_e} = \sqrt{1 - \frac{2\mu_0 p}{B_e^2}} .$$

Combining these two equations with (2) yields

$$af(\rho, 0) \approx \sqrt{1 - \frac{2\mu_0 p}{B_e^2}} - 1 .$$

The magnetosheath pressure p can be assumed to approximately equal the magnetic pressure just earthward from the magnetopause subsolar point. Assuming the total magnetic field there to be roughly twice that of the dipolar field at $\rho = \rho_s$ [e.g., *Mead and Beard*, 1964], we have $p \sim 2M_E^2/\mu_0\rho_s^6$, where M_E is the Earth's magnetic moment. In a crude approximation the background exterior field around the cusp at low and intermediate altitudes is $B_e \approx 2M_E/\rho^3$. From these estimates we obtain

$$af(\rho, 0) \approx \sqrt{1 - \left(\frac{\rho}{\rho_s}\right)^6} - 1 . \qquad (9)$$

Equation (9) becomes invalid near the "throat" of the outer cusp (i.e., for $\rho \sim \rho_s$), both because of the drastic change in the magnetic field geometry in that region (which invalidates the simplistic pressure balance considerations) and because of the breakdown of the dipolar approximation for B_e. However, it still should approximately hold at lower altitudes; owing to a rapid decrease of the term $(\rho/\rho_s)^6$, (9) provides a simple estimate of the radial variation of the field disturbance $\Delta B = B - B_e$ due to the cusp plasma:

$$\Delta B = B_e\, af(\rho, 0) \sim -\frac{B_e}{2}\left(\frac{\rho}{\rho_s}\right)^6 \approx -\left(\frac{M_E}{\rho_s^3}\right)\left(\frac{\rho}{\rho_s}\right)^3 . \qquad (10)$$

To put it in simple words, at low and intermediate distances, (10) predicts the diamagnetic disturbance inside the cusp to vary roughly as the cube of the radial distance, provided the plasma pressure in the entry region is isotropic. Turning to the plots of ΔB in Figures 2 and 4–6, one can see that the actual variation rate is somewhat slower: assuming the average distances for the plots in Figures 2 and 6 to be equal to 8.5 R_E and 5.5 R_E, respectively, one would expect from (10) a decrease of ΔB by a factor of 3.7, from the outer-

most to the innermost bin of the radial distance. At the same time, the observed change of the average ΔB, as it appears from the comparison of the plots, is significantly smaller, by a factor of ~ 2. A probable cause for that disagreement can be a field-aligned anisotropy of the pressure in the entry region, resulting from energization of the particles due to the merging of the geomagnetic field and the IMF [*Chen et al.*, 1998]. However, a more accurate investigation of the cusp depression is needed before making a definitive conclusion. As already noted, the values of ΔB obtained in this study could also have been affected by the inaccuracy of T96 model magnetopause near the cusps.

With the above in mind, we chose the factor $f(\rho, Y)$ in (2) in the form

$$f(\rho, Y) = \frac{\rho^\kappa}{\rho^\kappa + \rho_s^\kappa} \exp\left(-\frac{Y^2}{Y_c^2}\right), \tag{11}$$

in which the radial variation at low altitudes follows the power law $\sim \rho^\kappa$, but saturates at $\rho \geq \rho_s = 10\,R_E$, to avoid too strong unphysical distortion of the field near the magnetopause. A specific value of κ can be chosen between 5 and 6, where $\kappa = 5$ brings the variation rate closer to the observed one, while $\kappa = 6$ corresponds to the case of isotropic plasma in a static pressure balance with an external quasi-dipolar field.

The scale width of the cusp depression in the dawn-dusk direction, Y_c, was assumed to increase linearly with geocentric distance. This is what one would naturally expect in the region of a quasi-dipolar magnetic field at low and intermediate altitudes, while in the outer cusp, Y_c can increase more rapidly. However, because of lack of knowledge on the actual geometry of the distant cusp, we retained the linear dependence $Y_c = Y_{c0}(\rho/\rho_s)$ for the entire range of distances, with $Y_{c0} = 4\,R_E$, a tentative value based on the observed azimuthal extent of the polar cusp depression.

The parameter $\delta\phi$ in (4), defining the latitudinal extent of the cusp, is also a function of the radial distance, so that at ionospheric heights $\delta\phi$ drops down to a few degrees but becomes much wider in the outer cusp. Again, our approach was to use the dipolar approximation for low and intermediate altitudes and introduce a saturation in the distant region. The dipolar field lines diverge away from each other in the meridional planes approximately as $\sim \rho^{3/2}$, which implies $\delta\phi \sim \rho^{1/2}$. We therefore assumed

$$\delta\phi = \delta\phi_0 \frac{\rho^{1/2}}{\rho^{1/2} + \rho_s^{1/2}}. \tag{12}$$

The asymmetry parameter Θ, entering in (4), was empirically defined to have the form

$$\Theta = \frac{1}{2} - \Delta\Theta \frac{\rho^3}{\rho^3 + \rho_s^3}. \tag{13}$$

with $\Delta\Theta = 0.6$, so that at low altitudes the depression profile across the cusp is nearly symmetrical, while in the outermost region the magnetic field polarward from the cusp becomes more compressed than on the opposite side, to simulate the observed effect of the solar wind at high latitudes (Figures 2 and 3).

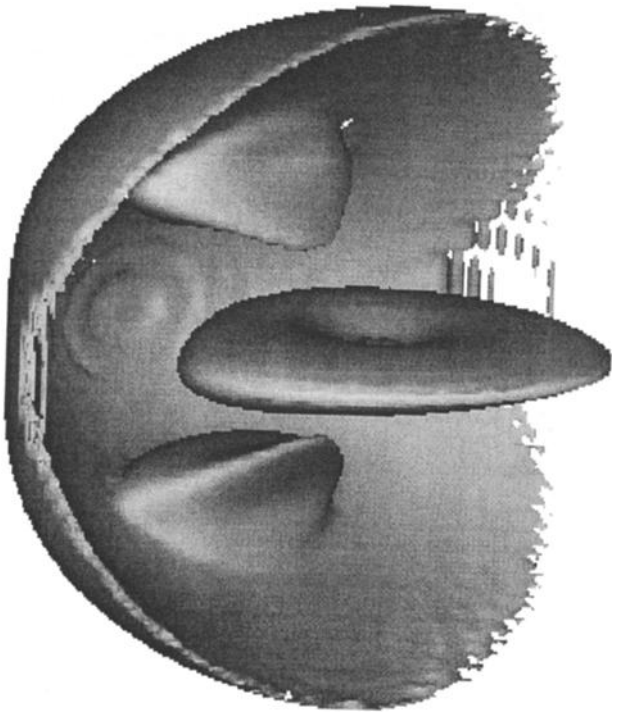

Figure 13. Three-dimensional view of the surface $\delta B = -10$ nT, illustrating the geometry of the model polar cusps. The toroidal surface near the equatorial plane is associated with the ring current depression.

3.2. Results

The outlined procedure was applied to a sample magnetosphere model in order to check the resultant distribution of the magnetic field and to compare the structure of the cusps in the model with the observations. The original (undeformed) field was represented by a simplified version of the T96 model, in which the field of the Region 1 and Region 2 Birkeland currents, unessential for the modeling of the polar cusp depression, were left out in order to speed up the calculations of the deformed field. The contribution from the Region 1 currents may shift the absolute latitudinal position of the cusps (defined via the angle ϕ_{c0} in (5)–(7)), but it results mostly in a transverse disturbance of **B** and hence does not significantly affect the magnitude of the field inside the cusps, which is the focus of this work. Another modification of the original T96 model was the adoption of a tilt-dependent shape of the nightside magnetopause, prompted by our recent finding made on the basis of the Geotail data [*Tsyganenko et al.*, 1998] and introduced into the model as described by *Tsyganenko* [1998].

Figure 12 displays four meridional profiles of the total model magnetic field in the noon plane, corresponding to centers of the four intervals of radial distance R, covered by the Polar data and discussed in section 2 (Figures 2, 4, 5, and 6). We note here that the amplitude of the polar cusp depression and other parameters were not fitted by least squares to the observed magnetic field. The purpose of this work is to present a method of incorporating the realistic cusps in the models, rather than to develop a comprehensive quantitative approximation to the existing data.

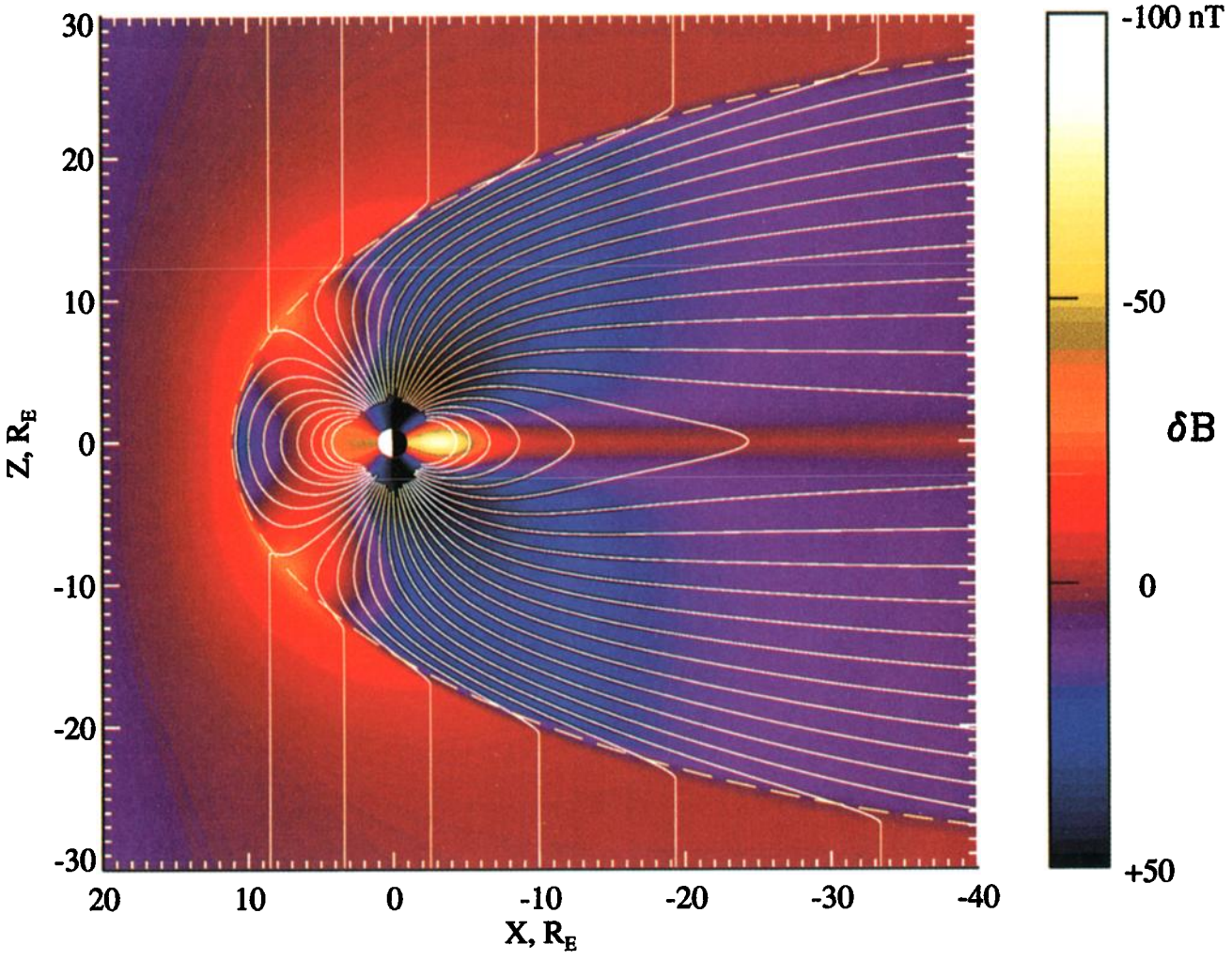

Plate 1. Color-coded plot of the difference $\delta B = B_{\text{model}} - B_{\text{dipole}}$ for the case of undeformed field (i.e., without the polar cusp effects).

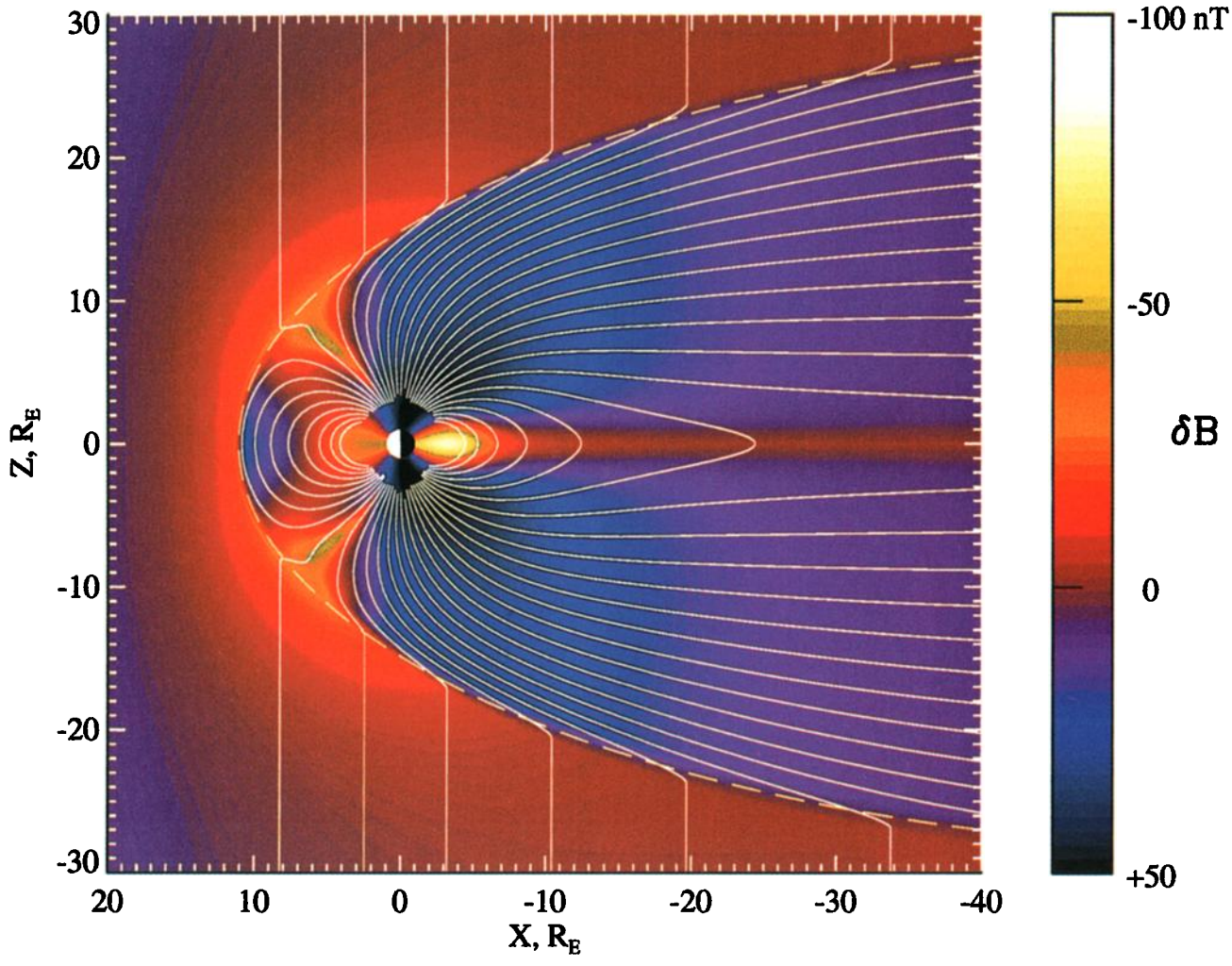

Plate 2. Color-coded plot of the difference $\delta B = B_{\text{model}} - B_{\text{dipole}}$, with the polar cusp depression, as defined in section 3.1. The northern and southern depressions are symmetrical owing to zero dipole tilt.

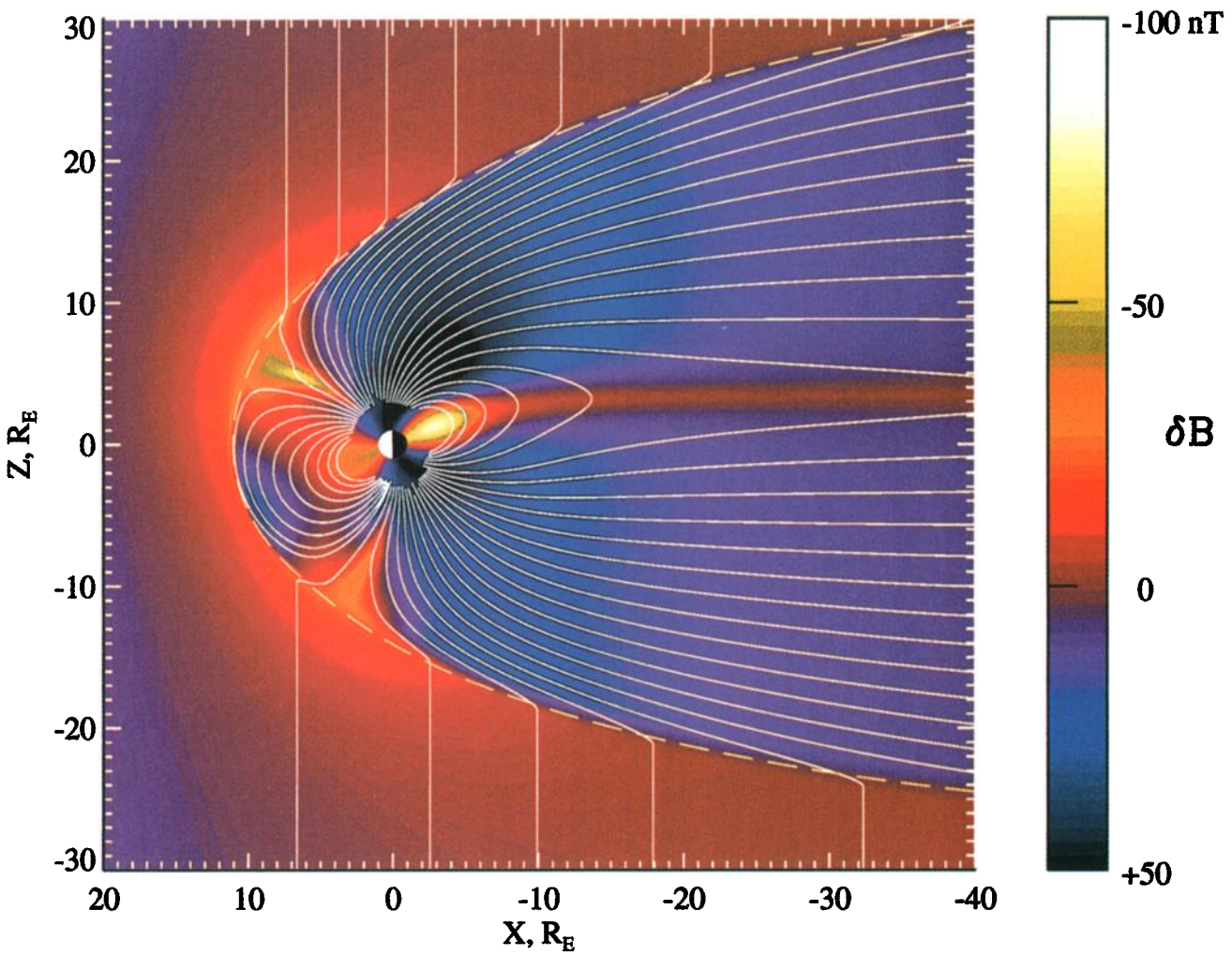

Plate 3. Color-coded plot of the difference $\delta B = B_{\text{model}} - B_{\text{dipole}}$, with the polar cusp depression, as defined in section 3.1, for a tilted Earth's dipole ($\Psi = 25°$). Owing to the greater exposure of the northern cusp to the solar wind flow, its magnetic field is more depressed than that in the southern cusp.

As originally intended, the model replicates both the localized depression at the latitudes $50° - 60°$ and the poleward region of compressed magnetic field at distances $R \geq 7\ R_E$. The amplitude of the depression decreases toward Earth; for the particular set of the cusp parameters used in generating the plots, ΔB varies from -33 nT at $R = 8.5\ R_E$ to -24 nT at $R = 5.5\ R_E$.

A simple and easy-to-grasp way to visualize the global pattern of a model magnetic field, including the polar cusp depressions, is to plot a distribution of the difference between the scalar magnitudes of the total model field and of the Earth's dipole field:

$$\delta B = |\mathbf{B}_{\text{mod}} + \mathbf{B}_{\text{dipole}}| - |\mathbf{B}_{\text{dipole}}| \tag{14}$$

(here we use the notation δB to distinguish it from the a different quantity, ΔB, discussed in section 2). Global maps of δB were first introduced by *Sugiura* [1971] for visualizing the global magnetospheric field as measured by OGO 3 spacecraft.

Plate 1 shows a color-coded pattern of δB for the original undeformed model field. In the low-latitude subsolar region and in the high-latitude nightside magnetosphere the model field is compressed relative to that of the dipole (blue and black colors), while inside the ring current and in the tail current sheet the field is depressed (yellow and red). In the vicinities of the two quasi-neutral points on the dayside magnetopause, there exist two broad regions of a moderately depressed field, but, since the original model does not feature the diamagnetic currents inside the cusps, there is no sharp depression like that observed in the data (Figures 2 and 4–6). On crossing the magnetopause, the model field abruptly drops down to relatively small values, and this is why the entire region outside the magnetosphere has a red color.

In Plate 2, the polar cusp depression was introduced by the deformation described in section 3.1. As a result, a conspicuous latitudinally narrow region with a significantly depressed field appears in the plot.

Plate 3 displays the effect of the Earth's dipole tilt on the position and relative intensity of the northern and southern cusp depression. Note, again, that the model cusp parameters were not fitted to data and that the purpose of the plots in Plates is just to demonstrate the method.

To illustrate the structure of the model cusps in three dimensions (3-D) and to visualize the longitudinal extension of the depressions, we plotted in Figure 13 a 3-D view of the surface $\delta B = -10$ nT. A toroidal structure in the middle is associated with the ring current depression, while the polar cusps appear as "tongues" extending down to Earth from the magnetopause. We again emphasize that the cusp features shown in Plates 1–3 and Figure 13 represent the magnetic field structure, rather than the plasma presence in the cusps, so the bright color-coded regions in Plates and the tongue-like feature in Figure 13 do not directly correspond to the plasma pressure distribution and should not be overinterpreted in this regard.

4. Concluding Remarks

We have studied the structure of the dayside magnetosphere on a basis of a large set of high-resolution data of Polar MFE and using a data-based magnetosphere model for detrending the data. A relatively narrow region of strongly depressed magnetic field was found in the vicinity of the expected position of the polar cusp field lines, extending down to geocentric distances of $\sim 5\ R_E$. In the outermost bin of the radial distance $8 \leq R < 9\ R_E$, clear evidence was found of a compressed magnetic field poleward from the cusp depression, which can be attributed to increased pressure of the magnetosheath plasma on the magnetopause, owing to a relatively large incidence angle of the flow in that region. The amplitude of the depression inside the cusps is clearly modulated by the tilt angle of the dipole, owing to an increase in the exposure of the summer hemisphere cusps to the incoming solar wind. Although somewhat larger depressions were observed for southward IMF conditions, the overall difference was not as dramatic as one might expect.

Using the magnetic field deformation method, a flexible model of the polar cusp diamagnetic depression was developed, allowing one to reproduce the observed field structure. The expected radial variation of the depression amplitude was derived, assuming isotropic pitch angle distribution of the injected particles and a static pressure balance across the polar cusp. Under that assumption the depression term should be proportional to the cube of the radial distance. The observed radial variation, however, was found to be slower, which may be due to a field-aligned anisotropy of the injected plasma, caused by a merging-related acceleration of particles along the field lines. Another possible cause for the discrepancy can be inaccurate approximation for the shape of the model magnetopause near the cusp "throat." A more detailed investigation of the role of the boundary currents in the cusp magnetic structure is relegated for a future study.

Finally, as already noted, no attempt has been made here to fit the cusp parameters to actual data. In the present model the position of the polar cusp depression is a free parameter, and it should be matched with the location of the neutral points at the magnetopause, which depends on the strength of major large-scale magnetospheric currents. In their turn, those currents are controlled both by the state of the solar wind and by the magnetospheric conditions, which means that the parameterization of the polar cusp model should be made in concert with that for the entire model. That task is also reserved for the further study, while the goal of the present work was to investigate the polar cusp depression using the data and develop a method for its mathematical representation.

Acknowledgments. We wish to thank the IMP 8 and Wind Magnetometer Data Processing Teams for the IMF data of those spacecraft, K. Ogilvie for providing the solar wind plasma data of Wind, and A. Lazarus for providing the solar wind plasma data of IMP 8. Thanks are due to T. Iyemori for providing the SYM and ASYM indices used in the detrending of the Polar data and to David

Stern for his many constructive comments on the first draft of the manuscript. The interplanetary medium data were retrieved using the NSSDC online facilities (SPYCAT and CDAWEB). This work is supported by NASA grants NASW-97024 (ISTP GI Program), and NSF Magnetospheric Physics Program grant ATM-9501463.

Hiroshi Matsumoto thanks M. Sugiura and S. Kokubun for their assistance in evaluating this paper.

References

Burch, J. L., Precipitation of low-energy electrons at high latitudes: Effects of interplanetary magnetic field and dipole tilt angle, *J. Geophys. Res., 77*, 6696, 1972.

Chapman, S., and V. C. A. Ferraro, A new theory of magnetic storms, *J. Geophys. Res., 36*, 77, 1931.

Chen, J., T. A. Fritz, R. B. Sheldon, H. E. Spence, W. N. Spjeldvik, J. F. Fennell, S. Livi, C. T. Russell, J. S. Pickett, and D. A. Gurnett, Cusp energetic particle events: Implications for a major acceleration region of the magnetosphere, *J. Geophys. Res., 103*, 69, 1998.

Fairfield, D. H., An evaluation of the Tsyganenko magnetic field model, *J. Geophys. Res., 96*, 1481, 1991.

Fairfield, D. H., and N. F. Ness, Imp 5 magnetic field measurements in the high-latitude outer magnetosphere near the noon meridian, *J. Geophys. Res., 77*, 611, 1972.

Farrell, W. M., and J. A. Van Allen, Observations of the Earth's polar cleft at large radial distances with the Hawkeye 1 magnetometer, *J. Geophys. Res., 95*, 20,945, 1990.

Mead, G. D., and D. B. Beard, Shape of the geomagnetic field solar wind boundary, *J. Geophys. Res., 69*, 1169, 1964.

Mead, G. D., and D. H. Fairfield, A quantitative magnetospheric model derived from spacecraft magnetometer data, *J. Geophys. Res., 80*, 523, 1975.

Newell, P. T., and C.-I. Meng, The cusp and the cleft/boundary layer: Low-latitude identification and statistical local time variation, *J. Geophys. Res., 93*, 14,549, 1988a.

Newell, P. T., and C.-I. Meng, Hemispherical asymmetry in cusp precipitation near solstices, *J. Geophys. Res., 93*, 2643, 1988b.

Newell, P. T., and C.-I. Meng, Dipole tilt effects on the latitude of the cusp and cleft/low-latitude boundary layer, *J. Geophys. Res., 94*, 6949, 1989.

Newell, P. T., C.-I. Meng, D. G. Sibeck, and R. P. Lepping, Some low-altitude cusp dependencies on interplanetary magnetic field, *J. Geophys. Res., 94*, 8921, 1989.

Russell, C. T., C. R. Chappell, M. D. Montgomery, M. Neugebauer, and F. L. Scarf, OGO 5 observations of the polar cusp on November 1, 1968, *J. Geophys. Res., 76*, 6743, 1971.

Russell, C. T., R. C. Snare, J. D. Means, D. Pierce, D. Dearborn, M. Larson, G. Barr, and G. Le, The GGS/Polar magnetic fields investigation, *Space Sci. Rev., 71*, 563, 1995.

Sandholt, P. E., C. J. Farrugia, P. Stauning, S. W. H. Cowley, and T. Hansen, Cusp/cleft auroral forms and activities in relation to ionospheric convection: Responses to specific changes in solar wind and interplanetary magnetic field conditions, *J. Geophys. Res., 101*, 5003, 1996.

Sotirelis, T., and C.-I. Meng, Magnetopause from pressure balance, *J. Geophys. Res., 104*, 6889, 1999.

Stern, D. P., Parabolic harmonics in magnetospheric modeling: The main dipole and the ring current, *J. Geophys. Res., 90*, 10,851, 1985.

Stern, D. P., Tail modeling in a stretched magnetosphere, 1, Methods and transformations, *J. Geophys. Res., 92*, 4437, 1987.

Sugiura, M., B. G. Ledley, T. L. Skillman, and J. P. Heppner, Magnetospheric field distortions observed by Ogo 3 and 5, *J. Geophys. Res., 76*, 7552, 1971.

Tsyganenko, N. A., A model of the cislunar magnetospheric field, *Ann. Geophys., 32*, 1, 1976.

Tsyganenko, N. A., Numerical models of quiet and disturbed geomagnetic field in the cislunar part of the magnetosphere, *Ann. Geophys., 37*, 381, 1981.

Tsyganenko, N. A., Quantitative models of the magnetospheric magnetic field: Methods and results, *Space Sci. Rev., 54*, 75, 1990.

Tsyganenko, N. A., Modeling the Earth's magnetospheric magnetic field confined within a realistic magnetopause, *J. Geophys. Res., 100*, 5599, 1995.

Tsyganenko, N. A., Effects of the solar wind conditions on the global magnetospheric configuration as deduced from data-based field models, *Eur. Space Agency Spec. Publ., ESA SP-389*, 181, 1996.

Tsyganenko, N. A., Modeling of twisted/warped magnetospheric configurations using the general deformation method, *J. Geophys. Res., 103*, 23,551, 1998.

Tsyganenko, N. A., and D. P. Stern, Modeling the global magnetic field of the large-scale Birkeland current systems, *J. Geophys. Res., 101*, 27,187, 1996.

Tsyganenko, N. A., and A. V. Usmanov, Effects of the dayside field-aligned currents in location and structure of polar cusps, *Planet. Space Sci., 32*, 97, 1984.

Tsyganenko, N. A., S. B. P. Karlsson, S. Kokubun, T. Yamamoto, A. J. Lazarus, K. W. Ogilvie, and C. T. Russell, Global configuration of the magnetotail current sheet as derived from Geotail, Wind, IMP 8, and ISEE 1/2 data, *J. Geophys. Res., 103*, 6827, 1998.

Tsyganenko, N. A., G. Le, C. T. Russell, and T. Iyemori, A study of the inner magnetosphere, based on data of Polar, *J. Geophys. Res., 104*, 10,275, 1999.

Walters, G. K., On the existence of a second standing shock wave attached to the magnetopause, *J. Geophys. Res., 71*, 1341, 1966.

White, W. W., G. L. Siscoe, G. M. Erickson, Z. Kaymaz, N. C. Maynard, K. D. Siebert, B. U. O. Sonnerup, and D. R. Weimer, The magnetospheric sash and the cross-tail S, *Geophys. Res. Lett., 25*, 1605, 1998.

Zhou, X.-W., C. T. Russell, G. Le, S. A. Fuselier, and J. D. Scudder, The polar cusp location and its dependence on dipole tilt, *Geophys. Res. Lett., 26*, 429, 1999a.

Zhou, X.-W., C. T. Russell, G. Le, S. A. Fuselier, and J. D. Scudder, Solar wind control of the polar cusp at high altitude, *J. Geophys. Res.*, in press, 1999b.

C. T. Russell, Institute of Geophysics and Planetary Physics, University of California, Los Angeles, 6877 Slichter Hall, Los Angeles, CA 90095-1567. (ctrussel@igpp.ucla.edu)

N. A. Tsyganenko, Code 690.2, Laboratory for Extraterrestrial Physics, NASA Goddard Space Flight Center, Greenbelt, MD 20771. (kolya@nssdca.gsfc.nasa.gov)

(Received March 10, 1999; revised June 21, 1999;
accepted June 22, 1999.)